# Refraction-Aware ADMM Reconstruction for Optical Projection Tomography of Multimaterial 3D-Print Filaments

Elise Yang

**Abstract**—Multimaterial 3D-printing, or multimaterial additive manufacturing (MMAM), harnesses the incredible ability to rapidly innovate with designs that can be highly customizable, complex, and multimaterial. However, a critical barrier impedes progress: current additive manufacturing (AM) process control methods are unable to visualize, verify, and correct internal 3D structures during the printing process. Overcoming this limitation would require a 3D imaging system that can be directly mounted on a 3D printer, and a volumetric reconstruction algorithm fast and precise enough to enable real-time feedback control. We thus seek to design a novel 3D reconstruction algorithm that can be coupled with a single-shot optical projection tomography (OPT) system. This algorithm must be capable of refraction-aware, high-speed, and sparse-view reconstructions. In this paper, we implement a refraction-aware reconstruction method with TV regularization for reconstructing semi-transparent materials from OPT, based on the Alternating Direction Method of Multipliers (ADMM). We demonstrate effectiveness on four simple cases relevant to rotating subvoxel-controlled extrusion-based MMAM. The method ultimately seeks to demonstrate a leap forward toward real-time, high-fidelity reconstructions for eventual adoption into MMAM process control pipelines with defect detection and feedback control for semi-transparent constructs.

**Index Terms**—Computational imaging, optical projection tomography, refraction-aware reconstruction, sparse-view tomography, ADMM, multimaterial additive manufacturing

## 1 Introduction

Multimaterial 3D-printing, or multimaterial additive manufacturing (MMAM), harnesses the incredible ability to rapidly innovate with designs that can be highly customizable, complex, and multimaterial. However, a critical barrier impedes progress: current additive manufacturing (AM) process control methods are unable to visualize, verify, and correct internal 3D structures during the printing process [1]. Overcoming this limitation would require a 3D imaging system that can be directly mounted on a 3D printer, and a volumetric reconstruction algorithm fast and precise enough to enable real-time feedback control. Such a system would enable 4D (3D + time) imaging of transparent and semi-transparent constructs. In particular, for extrusion-based MMAM, this could be used to image and reconstruct individual multimaterial filaments with "subvoxelated" internal features [2], enabling real-time quality control on the sub-filament level.

We thus seek to design a novel 3D reconstruction algorithm that can be coupled with a single-shot optical projection tomography (OPT) system. This algorithm must be capable of **refraction-aware**, **high-speed**, and **sparse-view reconstructions**: refraction-aware for handling nonlinear light paths through refractive materials, rapid for real-time reconstruction, and sparse-view for handling limited camera space and angles.

To address these requirements, we implement a refraction-aware reconstruction method with TV regularization for reconstructing semi-transparent materials from OPT, based on the Alternating Direction Method of Multipliers (ADMM). We demonstrate effectiveness on three simple cases relevant to rotating subvoxel-controlled extrusion-based MMAM. The method ultimately seeks to demonstrate a leap forward toward real-time, high-fidelity reconstructions for eventual adoption into MMAM process control pipelines with defect detection and feedback control.

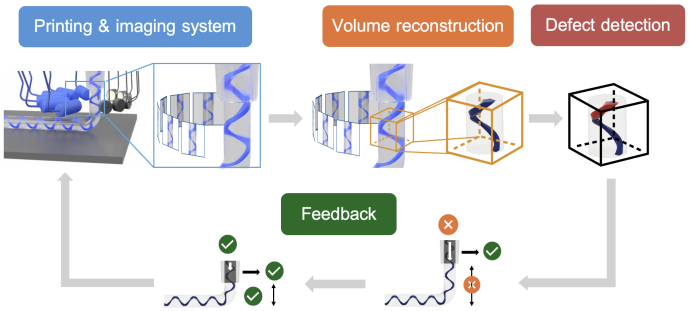


Fig. 1. 4D vision system pipeline for real-time operando guidance of extrusion-based MMAM.

## 2 Related Work

### 2.1 AM quality control methods

Current quality control methods for additively manufactured 3D structures, such as **layer-wise optical inspection**, **optical coherence tomography**, and **X-ray CT**, rely on sparsely sampled, interrupted, or post-fabrication imaging techniques, where correcting a defect is often no longer possible after its discovery [3], [4]. On the other hand, in-situ AM monitoring approaches, such as **thermal and acoustic**

• *E. Yang is with the Department of Mechanical Engineering, Stanford University, Stanford, CA, 94305.*
*E-mail: yelise@stanford.edu*

**imaging**, do not provide internal 3D structural information, limiting the ability to localize and correct defects in multi-material builds.

Optical projection tomography (OPT) has proven to be a compact, non-destructive imaging system that can be cheaply employed as a single-shot multi-camera system [5], [6]; it is thus an excellent candidate for an accessible, high-speed solution to image AM processes in operation. High-speed imaging alone, however, is not enough to provide rapid responses to make decisions in time—it must be paired with rapid volume reconstruction.

### 2.2 Volumetric reconstruction methods

There are various approaches that take a set of projection images and reconstruct them into a 3D representation. We focus on ones that relate to tomographic reconstruction and attempt to address at least one of the three following requirements for our application: refraction, high-speeds, and sparse-views.

#### *2.2.1 Refraction-aware reconstruction*

For OPT in particular, traditional methods in this area address refraction by submerging the sample in an index-matched fluid [5], [7]. This is not possible for imaging during printing.

Some novel view synthesis applications take advantage of known mathematical models of refractive light transparent using the Eikonal rendering to trace rays through differentiable refractive fields [8], [9].

#### *2.2.2 High-speed and sparse-view reconstruction*

Typically, traditional analytic tomographic reconstruction methods are slow to reconstruct 3D images and require hundreds of projection images. Both of these issues have been explored to be resolved by neural-based learning methods [10] [11]. However, these are application-dependent and require extensive training data.

Iterative algorithms have also proved to be effective in achieve higher speeds and reconstructing with sparse views [12]. In particular, ADMM-based methods have are effective for sparse view reconstruction and can incorporate physics priors and nonlinear models [13], [14]. Because ADMM is capable of incorporating multiple subproblems, its ability to be coupled with multiple priors, regularization terms, neural-based methods and nonlinear models could be a promising path forward for addressing all three requirements mentioned previously.

## 3 Proposed Method

We propose a refraction-aware ADMM-based method with TV regularization for reconstructing semi-transparent materials from OPT. Given a set of projection images, a refractive index field, and the number of materials, the algorithm returns a volume grid of absorption coefficients, providing the 3D structural information of each material.

### 3.1 Refraction-aware forward and inverse problem

#### *3.1.1 Forward problem*

A nonlinear, refraction-aware forward model is implemented in Pytorch using torchdiffeq to account for refractive deflections in OPT. The forward model maps a 3D voxel volume parameterized by spatially varying attenuation $\mu(r)$ and refractive index $n(r)$ to predicted projection images at arbitrary view angles. For a given projection angle $\theta$, each sensor pixel corresponds to a ray launched into the volume. Ray paths would be obtained by numerically integrating the Eikonal ray ODEs. The ray evolution is as follows in Eqs. (1) and (2):

$$\frac{d\mathbf{r}}{ds} = \mathbf{t} \tag{1}$$

$$\frac{d\mathbf{t}}{ds} = \nabla \ln n(\mathbf{r}) - (\mathbf{t} \cdot \nabla \ln n(\mathbf{r}))\,\mathbf{t} \tag{2}$$

where $\nabla \ln n(\mathbf{r}) = \frac{\nabla n(\mathbf{r})}{n(\mathbf{r})}$. $\mathbf{r}(s)$ is the ray position and $\mathbf{t}(s)$ is the unit direction, both parameterized by $s$.

With the ray trajectory r(s), the intensity accumulated along the path can be computed via the Beer-Lambert law:

$$\hat{I}_{\theta_i}(\mathbf{p}) = F(\mu, n, \theta_i) \tag{3}$$

$$= I_0 \exp\left(-\int \mu\big(\mathbf{r}_{\theta_i}(s;\mathbf{p})\big)\, ds\right) \tag{4}$$

Computing $\hat{I}_{\theta_i}(\mathbf{p})$ for each detector pixel given a projection angle $\theta_i$ gives us our forward model, where given a volume and its respective refractive index field ($n$-field), we can output an image that obeys the Eikonal mathematical model for refraction.

#### *3.1.2 Inverse problem*

The inverse problem is to recover $\mu$ from measured projection images $I_{\theta_i}(\mathbf{p})$. Since this problem is ill-posed, we formulate reconstruction as a regularized optimization problem:

$$\mu^* = \arg\min_{\mu} \sum_i \|F(\mu, n, \theta_i) - I_{\theta_i}\|_2^2 + \lambda\, \mathcal{R}(\mu), \tag{5}$$

where the first term enforces data fidelity and $\mathcal{R}(\mu)$ is a regularization term, such as total variation.

### 3.2 ADMM-based reconstruction model and optimization problem

To solve the inverse problem, we use the alternating direction method of multipliers (ADMM) with a total variation regularization (TV) term. Introducing an auxiliary variable $\mathbf{z} = D\mu$, where $D$ is the discrete gradient operator, we rewrite the reconstruction problem as

$$\min_{\mu,\mathbf{z}} \sum_i \left\|F(\mu, n, \theta_i) - I_{\theta_i}^{\text{meas}}\right\|_2^2 + \lambda\|\mathbf{z}\|_1 \quad \text{s.t.} \quad \mathbf{z} = D\mu. \tag{6}$$

The corresponding augmented Lagrangian is

$$\begin{aligned}\mathcal{L}_\rho(\mu, \mathbf{z}, \mathbf{u}) = &\sum_i \left\|F(\mu, n, \theta_i) - I_{\theta_i}^{\text{meas}}\right\|_2^2 + \lambda\|\mathbf{z}\|_1 \\ &+ \frac{\rho}{2}\left\|D\mu - \mathbf{z} + \mathbf{u}\right\|_2^2\end{aligned} \tag{7}$$

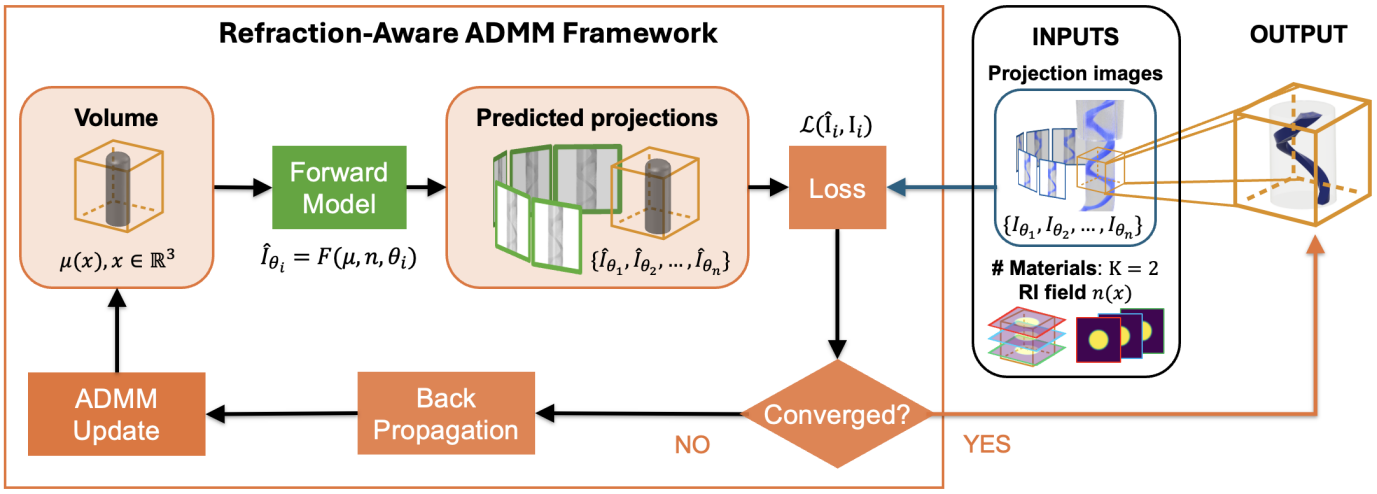


Fig. 2. Example two-column figure.

where $\mathbf{u}$ is the scaled dual variable and $\rho > 0$ is the penalty parameter.

At iteration $k$, ADMM performs the following updates:

$$\mu^{k+1} = \arg\min_{\mu} \sum_i \left\| F(\mu, n, \theta_i) - I_{\theta_i}^{\text{meas}} \right\|_2^2 + \frac{\rho}{2} \left\| D\mu - \mathbf{z}^k + \mathbf{u}^k \right\|_2^2 \tag{8}$$

$$\mathbf{z}^{k+1} = \arg\min_{\mathbf{z}} \ \lambda \|\mathbf{z}\|_1 + \frac{\rho}{2} \left\| D\mu^{k+1} - \mathbf{z} + \mathbf{u}^k \right\|_2^2 \tag{9}$$

$$\mathbf{u}^{k+1} = \mathbf{u}^k + D\mu^{k+1} - \mathbf{z}^{k+1}. \tag{10}$$

Here, the $\mu$-update enforces agreement with the measured projections through the nonlinear refraction-aware forward model, while the $\mathbf{z}$-update applies the TV prior to promote piecewise-smooth reconstructions. The dual update then enforces consistency between $\mathbf{z}$ and the image gradients $D\mu$.

## 4 Experimental Results

We experimented the algorithm on four different sets of projections, each with 36 projections of evenly spaced angles of 10 degrees across 360 degrees with resolution of 256 by 256 pixels. Three were rendered using the forward model from .obj files, and one was OPT images of a fabricated sample. These projections are to mimic extrusion-based MMAM with rotational subvoxel control. The four input sets are the following:

(a) Volumetrically rendered images of a cylinder.
(b) Volumetrically rendered images of single helix within cylinder.
(c) Volumetrically rendered images of double helix within same cylinder.
(d) A real set of images of the same structure as (b), fabricated with a clear resin-printed cylinder with RI=1.5 and injected with dyed pluronic gel through a helical void.

The cylinder and helices in (a)-(c) have an absorption value assigned to it to represent an absorbing material. In (d), we assume an absorption value of 0 for the cylinder since it was made of clear resin.

For all experiments, the $\mu$-update subproblem in ADMM was numerically solved using Euler integration with step size $ds = 2$ and optimized with ADAM. To accelerate computation, each iteration used a stochastic batch of 4 projections sampled from the full set of 36 views.

### 4.1 Choosing $\rho$ and $\lambda$

We first conducted a simple parameter sweep on the basic cylindrical model (a) to determine suitable values for the TV regularization weight $\lambda$ and ADMM penalty parameter $\rho$. The results are shown in Fig. 4. Based on PSNR, SSIM, and qualitative agreement with the ground truth in Fig. 3, we selected $\lambda = 0.1$ and $\rho = 100$ to use with our minimization problem. This choice was motivated in part by the ringing artifacts present in the cylinder-only reconstruction; thus, we favored parameters that reduced these artifacts while preserving the correct shape and absorption magnitude, without there being too much blur.

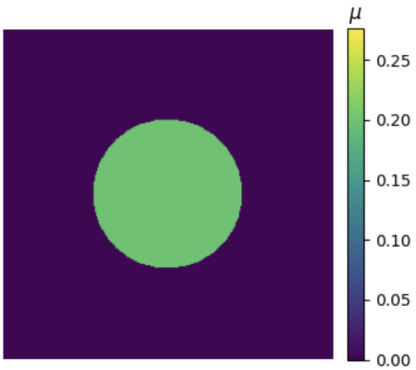


Fig. 3. Ground truth volume of (a) at mid-axial slice.

### 4.2 Results of case studies

### 4.3 Comparison to other methods

With $\lambda = 0.1$ and $\rho = 100$, we applied ADMM + TV to the four case studies. The reconstructions and selected

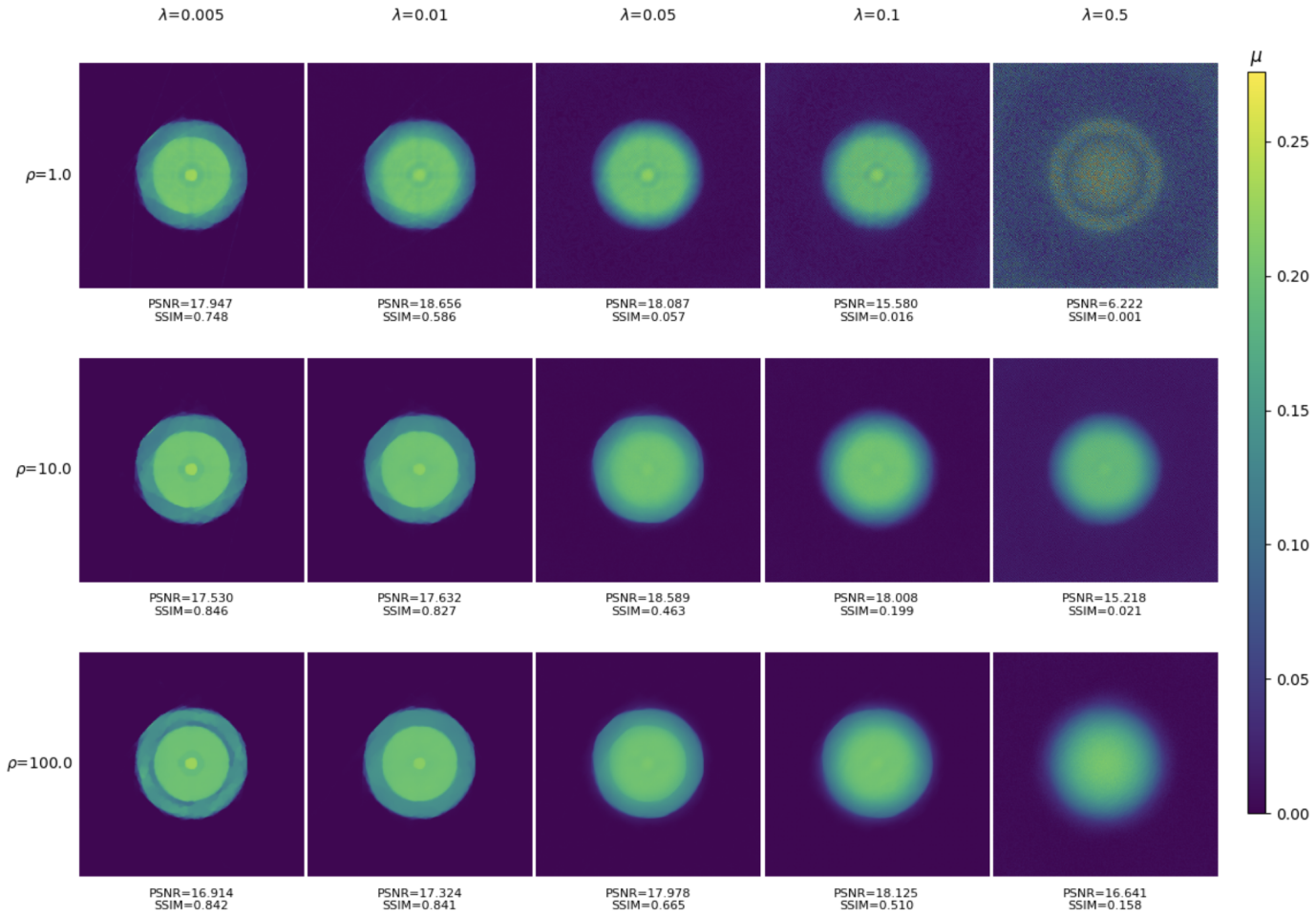


Fig. 4. Varying $\rho$ and $\lambda$ with mid-axial slice of ADMM + TV reconstruction of input (a).

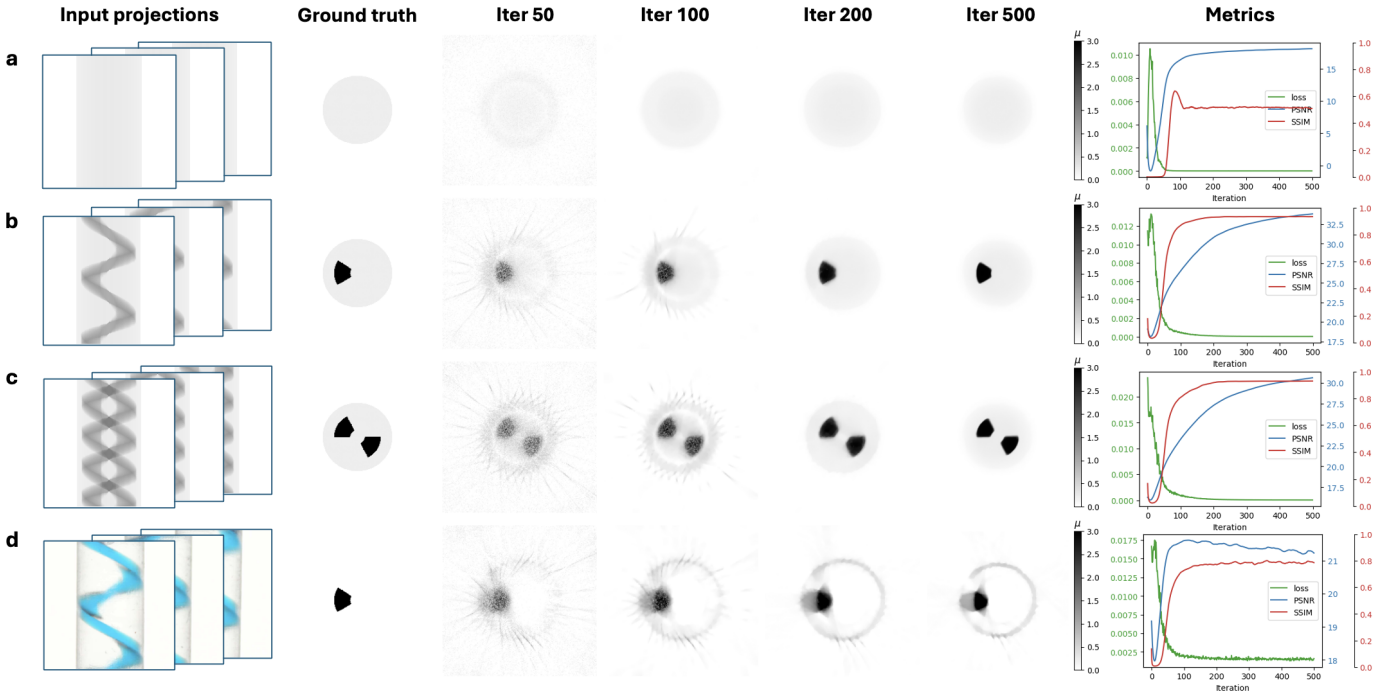


Fig. 5. Experimental results for the four input cases.

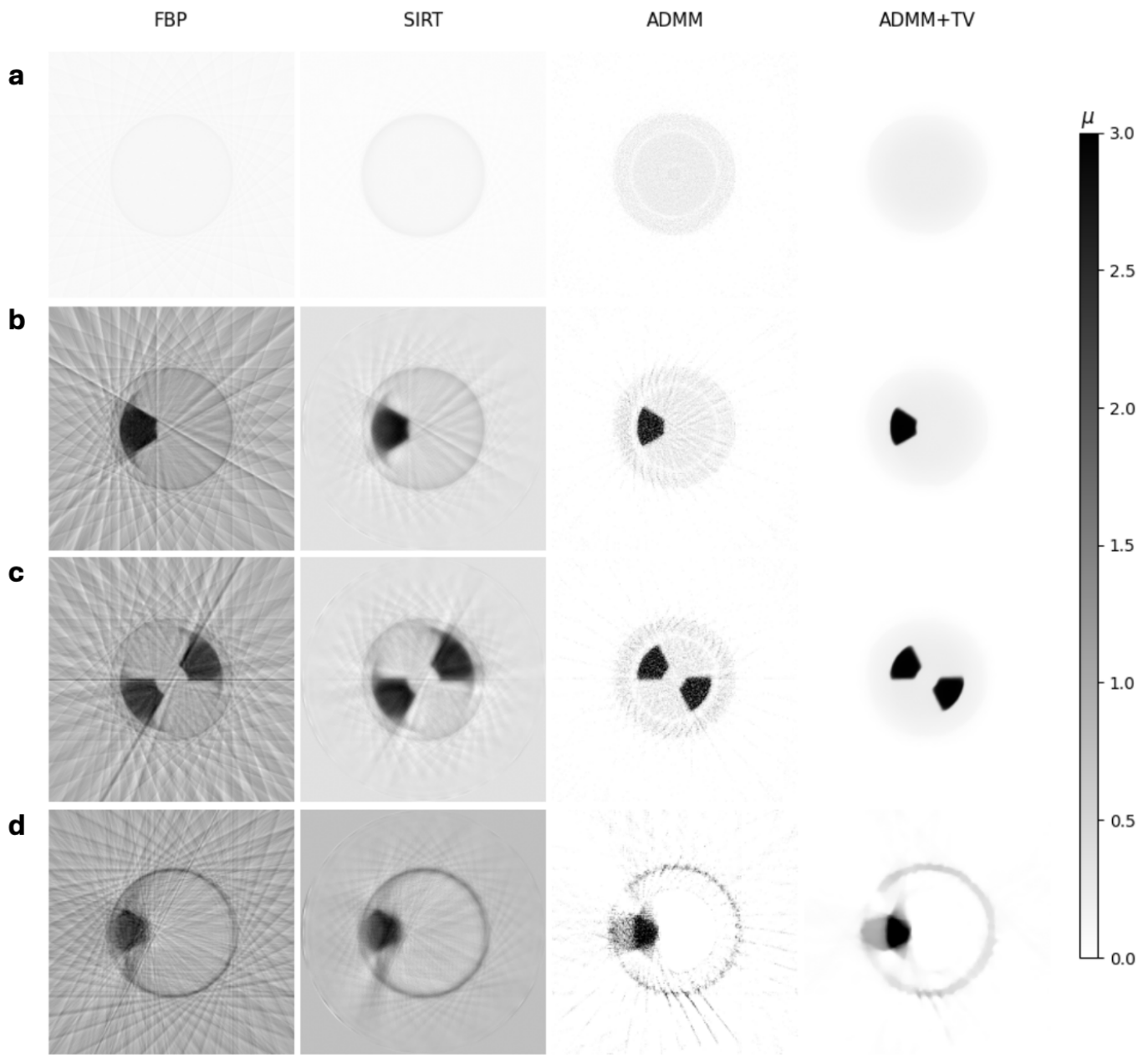


Fig. 6. Qualitative comparison of FBP, SIRT, ADMM, and ADMM + TV for the four reconstruction cases.

intermediate iterations are shown in Fig. 5. For the synthetic cases rendered with the forward model, SSIM improves rapidly and typically stabilizes within about 200 iterations. Although PSNR continues to improve more gradually for cases (b) and (c), the reconstructed structures are already visually close to the ground truth once SSIM approaches 1. For the these ADMM + TV reconstructions, 500 iterations required approximately 220 seconds. Since the synthetic cases typically reached good qualitative convergence within about 200 iterations, useful reconstructions could often be obtained in under 90 seconds.

The cylinder-only case in Fig. 5(a) still exhibits ringing artifacts, consistent with the observations from the parameter study. These artifacts reduce both PSNR and SSIM despite the overall cylindrical shape being recovered correctly.

For the single-helix and double-helix cases in Fig. 5(b)–(c), the method is able to recover the main internal geometry well, showing that the refraction-aware ADMM framework can reconstruct more complex multimaterial structures than a simple homogeneous cylinder.

The real fan-helix reconstruction in Fig. 5(d) is less accurate than the synthetic cases, but still captures the overall fan-shaped helical structure. One important limitation is that the ground-truth absorption values for this case were only estimated. In particular, the clear resin cylinder was assigned zero absorption, since it would ideally be nearly invisible in a rendering-based model. In the measured projections, however, the cylinder boundaries still appear darker due to real optical effects and modeling mismatch, for example by total internal reflection effects. This likely contributes to the darker edge artifacts seen in the reconstruction. Even so, the reconstruction maintains

| Case | FBP | | SIRT | | ADMM | | ADMM + TV | |
|---|---|---|---|---|---|---|---|---|
| | PSNR | SSIM | PSNR | SSIM | PSNR | SSIM | PSNR | SSIM |
| a | 7.7314 | 0.0840 | 10.3057 | 0.0838 | 10.3256 | 0.4159 | 18.1247 | 0.5101 |
| b | 10.2486 | 0.0246 | 16.9605 | 0.0675 | 26.2500 | 0.7835 | 33.8132 | 0.9339 |
| c | 9.3714 | 0.0119 | 12.6508 | 0.0309 | 23.7819 | 0.7678 | 30.6222 | 0.9301 |
| d | 9.1961 | 0.0011 | 11.2666 | 0.0030 | 19.2040 | 0.6456 | 21.2255 | 0.7849 |

TABLE 1
Quantitative comparison of reconstruction quality across the four test cases using FBP, SIRT, ADMM, and ADMM with TV regularization. PSNR and SSIM are reported for the reconstructed mid-slice relative to the ground-truth mid-slice.

reasonable structural fidelity, and SSIM converges steadily to approximately 0.8.

Overall, these case studies show that the proposed method can recover the dominant geometry of both simulated and real semi-transparent filament-like samples from only 36 projections, while also highlighting remaining challenges in artifact suppression and quantitative recovery for real data.

We compare our ADMM + TV method against filtered backprojection (FBP), the simultaneous iterative reconstruction technique (SIRT), and pure ADMM without TV regularization across all four cases. Qualitative results are shown in Fig. 6, and quantitative metrics are reported in Table 1.

Across all cases, FBP performs the worst visually and quantitatively. In the cylinder case in Fig. 6(a), FBP produces strong streak artifacts throughout the background and fails to cleanly recover the uniform boundary of the cylinder. In the more complex single-helix and double-helix cases in Fig. 6(b)–(c), these streaking artifacts become even more severe and obscure the internal absorbing structures. This is consistent with the low SSIM values of 0.0840, 0.0246, and 0.0119 for cases (a)–(c), respectively. In the real-data case, FBP also fails to isolate the helical feature and is dominated by backprojection streaks.

SIRT improves upon FBP by reducing some of the strongest streak artifacts, but the reconstructions remain blurry and still contain noticeable radial smearing. In case (a), SIRT recovers the circular boundary more cleanly than FBP, but still underestimates sharpness and contrast. In cases (b) and (c), the internal absorbing regions become more visible than in FBP, yet the boundaries are diffuse and the structures are not sharply separated from the surrounding cylinder. The quantitative metrics reflect this intermediate performance, with PSNR and SSIM consistently higher than FBP but still much lower than the ADMM-based approaches.

Both FBP and SIRT visibly also do not account for refractive effects—the helices are much farther placed than they should be due to refractive distortion. Their background is also unable to be resolved as with non-absorbing values.

Pure ADMM (with the refractive-aware forward model) performs substantially better than both FBP and SIRT in all four cases. In the synthetic examples, ADMM clearly recovers the locations and approximate shapes of the absorbing internal structures, demonstrating the benefit of using the refraction-aware forward model in the reconstruction process. However, without TV regularization, the results remain noisy and exhibit grainy edge artifacts, especially in the cylinder-only case and around the boundaries of the internal features in cases (b) and (c). This is particularly visible in Fig. 6, where ADMM captures the correct geometry but leaves substantial speckled texture and residual star-like artifacts.

ADMM + TV gives the best overall performance both visually and quantitatively. In the synthetic cases, it most accurately recovers the intended piecewise-smooth structures, producing the cleanest material boundaries and the least amount of background artifact. In case (a), TV regularization strongly suppresses the ringing and speckle seen in pure ADMM while preserving the circular cylinder shape. In cases (b) and (c), ADMM + TV yields the sharpest and most compact reconstructions of the internal absorbing regions, with PSNR/SSIM improving from 26.2500/0.7835 to 33.8132/0.9339 in case (b), and from 23.7819/0.7678 to 30.6222/0.9301 in case (c). In the real-data case, ADMM + TV also produces the clearest reconstruction of the internal feature, while still showing some residual mismatch at the cylinder boundary that likely arises from modeling error and unmodeled optical phenomena.

Overall, these comparisons show that the main performance gain comes from combining a refraction-aware nonlinear forward model with TV regularization. Traditional tomographic methods such as FBP and SIRT are not well suited to this problem because they do not account for refracted ray paths and are highly sensitive to sparse-view artifacts. Refraction-aware ADMM already provides a major improvement, and adding TV regularization further improves material localization, suppresses noise, and yields the highest-fidelity reconstructions among all methods tested.

## 5 Conclusion

In this work, we presented a refraction-aware ADMM reconstruction framework with TV regularization for optical projection tomography of multimaterial 3D-print filaments. Across four case studies, the method was able to recover the dominant internal structure of both simulated and real semi-transparent samples using only 36 evenly spaced projections, demonstrating the promise of combining nonlinear refractive physics with iterative sparse-view reconstruction.

The experiments, still, reveal several opportunities for future improvement. For example, further optimization of reconstruction parameters and update schemes could improve material separation and reduce artifacts such as ringing, leading to clearer and more correct distinction between neighboring materials. Additionally, the current formulation reconstructs only a scalar absorption field. Extending the forward and inverse model to include RGB color or wavelength-dependent attenuation would provide richer

contrast and could improve differentiation between materials that are difficult to separate with absorption alone. We would also eventually want to learn the $n$-field as well in case filaments, as they are printing, deviate from the expected path. Furthermore, while 36 projections already represents a relatively sparse setting compared to many traditional tomographic methods, future work should further stress-test the framework under even fewer views to better characterize its sparse-view limits. Finally, we have not reached "real-time" speeds yet, given that at 200 iterations we are just under a 90 second reconstruction time. Further exploration in improving computational efficiency such as exploring other priors and embedding a neural network could help.

Overall, the results suggest that refraction-aware ADMM is a promising step toward fast, sparse-view OPT reconstruction for eventual real-time multimaterial additive manufacturing process monitoring and feedback control.

## Acknowledgments

The author would like to thank the teaching staff of EE367, especially Professor Gordon Wetzstein and course assistant Sonia Kim, for their guidance and support throughout the quarter. The author also thanks Professor Natalie Larson and Professor Eric Darve for research mentorship and support.

## References

[1] S. A. M. Tofail, E. P. Koumoulos, A. Bandyopadhyay, S. Bose, L. O'Donoghue, and C. Charitidis, "Additive manufacturing: scientific and technological challenges, market uptake and opportunities," *Materials Today*, vol. 21, no. 1, pp. 22–37, Jan. 2018.

[2] N. M. Larson, J. Mueller, A. Chortos, Z. S. Davidson, D. R. Clarke, and J. A. Lewis, "Rotational multimaterial printing of filaments with subvoxel control," *Nature*, vol. 613, no. 7945, pp. 682–688, Jan. 2023.

[3] J. W. Tashman *et al.*, "In situ volumetric imaging and analysis of fresh 3d bioprinted constructs using optical coherence tomography," *Biofabrication*, vol. 15, no. 1, Oct. 2022.

[4] A. Thompson, I. Maskery, and R. K. Leach, "X-ray computed tomography for additive manufacturing: a review," *Measurement Science and Technology*, vol. 27, no. 7, p. 072001, Jun. 2016.

[5] J. Sharpe, "Optical projection tomography as a new tool for studying embryo anatomy," *Journal of Anatomy*, vol. 202, no. 2, pp. 175–181, 2003.

[6] C. Darling, S. P. X. Davis, S. Kumar, P. M. W. French, and J. McGinty, "Single-shot optical projection tomography for high-speed volumetric imaging of dynamic biological samples," *Journal of Biophotonics*, vol. 16, no. 2, p. e202200232, Feb. 2023.

[7] B. Trifonov, D. Bradley, and W. Heidrich, "Tomographic reconstruction of transparent objects," in *Proceedings of the Eurographics Symposium on Rendering*, 2006, pp. 51–60.

[8] X. Chen, J. Liu, H. Zhao, G. Zhou, and Y.-Q. Zhang, "Nerrf: 3d reconstruction and view synthesis for transparent and specular objects with neural refractive-reflective fields," *arXiv preprint arXiv:2309.13039*, 2023.

[9] I. Ihrke, G. Ziegler, A. Tevs, C. Theobalt, M. Magnor, and H.-P. Seidel, "Eikonal rendering: Efficient light transport in refractive objects," *ACM Transactions on Graphics*, vol. 26, no. 3, p. 59, 2007.

[10] E. M. Asimakopoulou, V. Bellucci, S. Birnsteinova, Z. Yao, Y. Zhang, I. Petrov, C. Deiter, A. Mazzolari, M. Romagnoni, D. Korytar, Z. Zaprazny, Z. Kuglerova, L. Juha, B. Lukic, A. Rack, L. Samoylova, F. Garcia-Moreno, S. A. Hall, T. Neu, X. Liang, P. Vagovic, and P. Villanueva-Perez, "Development towards high-resolution khz-speed rotation-free volumetric imaging," *Optics Express*, vol. 32, no. 3, pp. 4413–4426, 2024.

[11] J. Sun, F. Zhao, L. Zhu, B. Liu, and P. Fei, "Optical projection tomography reconstruction with few views using highly-generalizable deep learning at sinogram domain," *Biomedical Optics Express*, vol. 14, no. 12, pp. 6260–6270, Dec. 2023.

[12] H. Chen, X. Ma, and J. Wang, "Comparison of reconstruction methods for optical projection tomography with sparse angle projections," in *International Conference on Optics and Machine Vision, ICOMV 2024*, ser. Proceedings of SPIE, vol. 13179, 2024, p. 1317918.

[13] C. Zhao, M. Ge, X. Yang, Y. S. Chu, and H. Yan, "Limited-angle x-ray nano-tomography with machine-learning enabled iterative reconstruction engine," *npj Computational Materials*, vol. 11, p. 240, 2025.

[14] J. Tao, Y. Wei, and B. Bo, "An admm method for diffuse optical tomography with l2 and l regularization," in *Fourth International Conference on Computer Graphics, Image, and Virtualization (ICCGIV 2024)*, ser. Proceedings of SPIE, vol. 13288, 2024.

**Elise Yang** Elise Yang is a first-year Mechanical Engineering PhD student at Stanford University.